ORCA – Online Research @ Cardiff

This is an Open Access document downloaded from ORCA, Cardiff University's institutional repository:https://orca.cardiff.ac.uk/id/eprint/173592/

This is the author's version of a work that was submitted to / accepted for publication.

Citation for final published version:

Xu, Yang, Lin, Dong, Zong, Ze, He, Qiuming, Ma, Zhe, Deng, Xuliang, Chen, De, Yang, Chaohe and Feng, Xiang 2024. Ammonia-regulated dynamic evolution of Ti precursor incorporating into dealuminized beta for efficient 1-Hexene epoxidation. Chemical Engineering Science 300 , 120594. 10.1016/j.ces.2024.120594

Publishers page: http://dx.doi.org/10.1016/j.ces.2024.120594

Please note:
Changes made as a result of publishing processes such as copy-editing, formatting and page numbers may not be reflected in this version. For the definitive version of this publication, please refer to the published source. You are advised to consult the publisher's version if you wish to cite this paper.

This version is being made available in accordance with publisher policies. See http://orca.cf.ac.uk/policies.html for usage policies. Copyright and moral rights for publications made available in ORCA are retained by the copyright holders.

Ammonia-regulated dynamic evolution of Ti precursor incorporating into dealuminized beta for efficient 1-Hexene epoxidation

Yang Xu [a,1], Dong Lin [b,1,*], Ze Zong [a], Qiuming He [a], Zhe Ma [a], Xuliang Deng [a], De Chen [c], Chaohe Yang [a], Xiang Feng [a,*]

[a] State Key Laboratory of Heavy Oil Processing, China University of Petroleum, Qingdao 266580, China
[b] Max Planck- Cardiff Centre on the Fundamentals of Heterogeneous Catalysis FUNCAT, Cardiff Catalysis Institute, School of Chemistry, Cardiff University, Cardiff, CF24 4HQ, United Kingdom
[c] Department of Chemical Engineering, Norwegian University of Science and Technology, Trondheim 7491, Norway

A R T I C L E I N F O

Keywords:
Ammonia-regulated evolution
Ethoxylated chlorotitanate precursor
framework Ti species
Ti-beta
1-Hexene epoxidation

A B S T R A C T

Demetalation-metalation method has gained prominence for its higher metal loading, efficiency and shortened synthetic period, particularly in the incorporation of metal atoms with large radii into zeolite framework in recent years. An ammonia-regulated approach has been developed for selectively evolved deep-substituted Ti precursors in dealuminized beta zeolites, which enables a controlled promotion of metalation of Ti atoms. Additionally, this ammonia-regulated approach could also enhance 1-hexene kinetic adsorption by constructing mesopores, which is demonstrated by the lower reaction order of 1-hexene. The synthesized ammonia-regulated N-Ti-beta exhibits rich framework Ti species and a high specific surface area, leading to significantly improved 1-hexene epoxidation performance (conversion of 61%, selectivity of 98%, and a high H_2O_2 utilization efficiency of 93%). This study not only provides a new strategy to dynamically regulate evolution of Ti precursors by ammonia but also holds promise for advancing related industrial processes in demetalation-metalation methods.

1. Introduction

Titanosilicate is regarded as a pivotal advancement in zeolite catalysis due to its distinctive oxidative prowess in various reactions, including alkene epoxidation, ketone ammoximation, alkane oxidation, oxidative desulfurization, aromatic hydroxylation, as well as the oxidation of alcohols and amines (Gordon et al., 2020; Lin et al., 2023a; Zhao et al., 2023). Notably, the application of this method to 1-hexene epoxidation for synthesizing 1,2-epoxyhexane is gaining prominence, owing to the substantial industrial significance of 1,2-epoxyhexane (Liang et al., 2023; Yuan et al., 2023; Zhang et al., 2021). This compound is widely employed in the production of disinfectants, hydrophobic polyethers, and polyols derived from ethers (Darensbourg, 2007; Hirahata et al., 2008). The dealumination-metalation method for preparing titanosilicates has attracted considerable attention for its straightforward synthetic process and high metal loading in alkene epoxidation (Bregante et al., 2018; Potts et al., 2022; Suib et al., 2022; Tan et al., 2022; Tang et al., 2014; Zhang et al., 2022).

Compared with traditional hydrothermal and dry-gel conversion methods, the demetalation-metalation method is gaining prominence, due to its numerous advantages, including high metal loading, efficient synthetic periods, and the incorporation of metal atoms with a large radius (Bregante and Flaherty, 2017; Li and Yu, 2021; Zhang et al., 2022). The demetalation-metalation process involves two key steps: demetallation of as-synthesized zeolites and subsequent metalation. In the demetallation of zeolites, the common zeolite types (e.g., silicate, borosilicate, germanosilicate, and aluminosilicate zeolites) require desilication, deboronation, degermanation, and dealumination, respectively (Dijkmans et al., 2013; Pang et al., 2021; Rodríguez-Ferna´ndez et al., 2020; Yamagishi et al., 1991). Then, lattice vacant sites are created by removing Si, Al, B, or Ge atoms through acidic or alkaline treatments (Liu et al., 2018; Song et al., 2017; Wolf et al., 2014). Sub- sequently, metal atoms with suitable radii react with hydroxyl nets within the zeolite framework at high temperatures, thereby facilitating the integration of metal atoms into the zeolite structure through an "atom-planting" process (Deng et al., 2023; Ge et al., 2023; Meng et al., 2024). Hence, the development of a novel strategy for titanosilicalite synthesis based on demetallation-metalation process for highly efficient

* Corresponding authors.
E-mail addresses: LinD6@cardiff.ac.uk (D. Lin), xiangfeng@upc.edu.cn (X. Feng).
[1] These authors contributed equally to this work.

1-hexene epoxidation becomes imperative.

In this study, an ammonia-regulated approach was employed to finely regulate the evolution of ethoxylated chlorotitanate ($Ti(Cl)_{4-n}(OEt)_n$) species and the subsequent Ti-incorporation process within dealuminized beta zeolites for 1-hexene epoxidation. The formation of ethoxylated chlorotitanate ($Ti(Cl)_{4-n}(OEt)_n$) and HCl species arises from the equilibrium reaction between chlorotitanate precursors ($TiCl_4$) and ethanol. Ammonia, in turn, reacts with HCl to generate NH_4Cl which could be precipitated from ethanol, disrupting the reaction equilibrium and facilitating the substitution of Cl in chlorotitanate by ethanol. The resulting deeply substituted Ti precursor proves highly effective in restraining the formation of TiO_x and extra-framework TiO_2 species. Moreover, the evaporation of NH_3 induces the creation of mesopores at optimized reaction conditions, thereby enhancing the kinetic adsorption of macromolecular 1-hexene. The synthesized ammonia-regulated Ti-beta material exhibits rich framework Ti species and more accessible Ti active sites, leading to a significantly improved performance in 1-hexene epoxidation.

2. Experimental section

2.1. Dealumination-Metallization process of Ti-beta.

Ti-beta zeolites were synthesized employing a dealumination-metallization strategy. In a standard synthesis procedure, 10 g of deal-

Co., Ltd) underwent calcination at 550 °C for 6 h, resulting in clean uminized H-beta zeolite (Zhuoran Environmental Protection (Dalian) dealuminized H-beta zeolites featuring nested silanol sites. For the incorporation of Ti, an appropriate quantity of $TiCl_4$ (99.9 %, Macklin) was initially blended with anhydrous ethanol to form the Ti precursor. Subsequently, 2 g of H-beta was introduced into the 10 mL of the Ti precursor, and the ensuing mixture was further ground. The final products were gathered and subjected to drying at 100 °C for 2 h, followed by calcination at 550 °C for 3 h. These resulting samples were designated as Ti-beta.

2.2. Dealumination-Metallization process of Ti-beta regulated by NH_3.

The synthesis procedure mirrored the aforementioned method, with the only variation being the placement of the ammonia solution during Ti incorporation. In this modified process, the 20 ml beaker containing Ti precursor was positioned at the base of a 500 ml glass beaker submerged in a water bath, featuring magnetic stirring. Additionally, ammonia solution (Sinopharm Chemical Reagent Co., Ltd) was introduced into the 500 ml glass beaker before carefully sealing it. The beaker serves as a barrier, preventing direct contact between the ammonia and the Ti precursor. In this setup, the ammonia can only vaporize, reaching the Ti precursor through gaseous interaction. Following stirring at specific temperature and 500 rpm for specific time, the resulting solid underwent treatment through drying at 110 °C for 2 h and subsequent calcination at 550 °C for 3 h. Ti-beta zeolites with different treatments were prepared by adjusting the processing temperature, time, and ammonia solution concentration. These catalysts were identified as Ti-beta-x°C, Ti-beta-yh, and Ti-beta-z, where x denotes the temperature, y represents the time, and z signifies the concentration of the ammonia solution (ml NH_3/[ml NH_3 + ml H_2O]).

2.3. Characterizations

The Ti species in Ti-beta were identified using ultraviolet–visible spectroscopy (UV–vis, Shimadzu UV-2700) after drying in ovens at 100 °C for 8 h, with pure $BaSO_4$ serving as the background. To capture the signals, the TS-1 sample was pressed against a $BaSO_4$ background and utilized with an integrating sphere accessory to enhance signal reflection. The relative percentages of the framework Ti species among all Ti species were calculated using the Gaussian fitting method, which included three Gaussian profiles: anatase TiO_2 species at 320 nm, hexagonal Ti species at 260 nm, and tetrahedral Ti species at 220 nm. The chemical composition of the samples was analyzed by ICP-OES (Agilent 730 inductively coupled plasma emission spectrometry). Fourier- transform infrared (FT-IR) spectrometer (Nicolet NEXUS 670) was

materials were heated to 500 °C at 10 °C·min^{-1} and held for 1 h under employed to investigate the framework structure of Ti-beta zeolites. All flowing air in the furnace to remove water and residual organics. Then, the samples, pressed into self-supporting disks (25 mg) with KBr (75

framework vibration region of Ti-beta zeolites were recorded at 25 °C. mg), were placed within the transmission cell. FT-IR spectra in the The chemical state of Ti species was determined by X-ray photoelectron

spectroscopy (XPS, Escalab 250Xi), with the C_1 binding energy serving as the reference. The pore structure of catalysts was assessed at 77 K using a volumetric adsorption analyzer (Micromeritics ASAP 2460). High-resolution transmission electron microscope (HRTEM) images of TS-1 crystals were obtained using a JEOL JSM-2100F microscope. Chemicals released during the calcination of uncalcined solid materials were analyzed by the TG-MS. Initially, the internal atmosphere of TGA

initial steady state, the sample was heated at a rate of 10 °C/min from ambient temperature to 800 °C, and the gas components were simulta-was flow air, and the flow rate was set to 50 mL/min. After a 30-minute neously detected and analyzed by mass spectrometry.

2.4. Catalytic testing

The synthesized Ti-beta zeolites were evaluated in the 1-hexene

a temperature of 60 °C. The reaction conditions were as follows: 0.2 g of epoxidation. All reactions were conducted in a 50 ml microreactor at catalyst, 1.2 g of 1-hexene (AR, Aladdin), 1.2 g of H_2O_2 (>30 wt%, Sinopharm Chemical Reagent Co., Ltd.), and 20 ml of CH_3CN (AR,

maintained at 60 °C for three hours under stirring at a speed of 300 rpm. Sinopharm Chemical Reagent Co., Ltd.). The reaction temperature was The resulting solution was transferred to a transparent sample vial containing anhydrous sodium sulfate and homogenously mixed to eliminate residual water. The H_2O_2 analysis was performed prior to the addition of sodium sulfate, ensuring that it did not influence the determination of H_2O_2 content. The supernatant was then collected, and 1 mL of the sample was extracted under continuous stirring and filtered into a chromatographic vial for analysis. The H_2O_2 utilization efficiency was verified using the Iodometric method. The procedure of H_2O_2 decomposition with Ti-beta catalysts is as follows: after 12 h of drying for the

20 ml CH_3CN, and the reaction is carried out for 3 h at 60 °C. catalysts, 1.2 g of H_2O_2 is carefully mixed with 0.2 g of Ti-beta catalyst in

The reaction products were quantified using gas chromatography (Agilent 7820A with an autosampler and HP-5 30 m × 320 μm × 0.25 μm) equipped with an FID detector. 1-Hexene conversion and product selectivity were determined based on the standard lines of the corresponding materials.

Elimination of the external diffusion limitations: To mitigate the impact of external diffusion, the stirring speed of the batch reactor is elevated. As illustrated in Fig. S1, at a consistent reaction time, the conversion rate of 1-hexene demonstrates an upward trend with increasing stirring speed. Beyond 300 r/min, however, the conversion rate of 1-hexene shows no significant further change, suggesting the effective elimination of external diffusion influence at this speed. Consequently, under the kinetic test conditions for catalyst evaluation, the stirring speed is set to 300 r/min.

Elimination of the internal diffusion limitations: Concerning internal diffusion, when the Wesiz modulus stays below 1.5, its influence on kinetics is deemed negligible. In this study, the Ti-beta catalyst features a grain size of approximately 0.4 μm, yielding a corresponding Wesiz modulus of about 0.015 below the 1.5 threshold. Consequently, it can be inferred that the evaluation system for 1-hexene epoxidation operates unaffected by internal diffusion.

$$\hat{I}_I = \frac{(p/6)^2 \times R_0}{D_{eff} \times C_0} \tag{1.1}$$

For the quantitative analysis of hydrogen peroxide using the iodometric method, 0.300 g of pre-reaction and post-reaction solutions were accurately weighed in an iodometric flask. Subsequently, 20 wt% H_2SO_4 solution was added to the flask. Saturated ammonium molybdate solution was added dropwise (approximately 1 mL), followed by the addition of 2 mL of 10 wt% KI solution. Then the flask was sealed in a dark environment for 20 min. Afterward, add 0.1 mol/L $Na_2S_2O_3$ solution dropwise to the mixture until the color becomes lighter. Subsequently, 2 mL of starch solution was introduced as an indicator. The addition of $Na_2S_2O_3$ solution was then continued until the solution turned colorless, indicating the conclusion of the titration process.

The reactants and products were calibrated to calculate conversion and selectivity values. For instance, the concentration of 1,2-epoxyhexane was determined using its standard curve at various concentrations, with m-xylene serving as the internal standard. The moles of reactants and products were derived from their respective standard curves. The conversion of 1-hexene and the selectivity of different products were determined as follows:

$$C(\%) = \frac{n_{before} - n_{after}}{n_{before}} \times 100\% \tag{1.2}$$

$$S(\%) = \frac{n_{1,2\text{-epoxyhexane}}}{n_{1,2\text{-epoxyhexane}} + n_{n\text{-pentanal}} + n_{1,2\text{-hexanediol}}} \times 100\% \tag{1.3}$$

$$TON = \frac{n_{1,2\text{-epoxyhexane}}}{n_{Ti}} \tag{1.4}$$

Herein, C represents the conversion of 1-hexene, S denotes the selectivity of each component in the product, n_{before} stands for the initial molar amount of 1-hexene, n_{after} signifies the molar amount of 1-hexene remaining in the solution at the end of the reaction, and n_{Ti} is the molar amount of titanium within the catalysts, which was determined through ICP-OES analysis.

The titration results were analyzed, where the hydrogen peroxide concentration was calculated as follows:

$$H_2O_2\ (wt\%) = \frac{34.016 \times 0.1 \times V}{2 \times W \times 1000} \times 100\% \tag{1.5}$$

where V is the volume of sodium thiosulfate solution consumed, and W is the mass of the weighed reaction solution.

The conversion of H_2O_2 and the effective utilization rate were calculated as follows:

$$X_{H_2O_2}(\%) = \frac{n^{before}_{H_2O_2} - n^{after}_{H_2O_2}}{n^{before}_{H_2O_2}} \times 100\% \tag{1.6}$$

$$Eff.(H_2O_2)(\%) = \frac{C(\%)}{X_{H_2O_2}(\%)} \times 100\% \tag{1.7}$$

Where $n^{before}_{H_2O_2}$ is the initial molar concentration of H_2O_2, $n^{after}_{H_2O_2}$ is the molar concentration of the remaining H_2O_2, C is the conversion of 1-hexene.

3. Results and discussion

3.1. Ammonia-regulated Ti precursor incorporated into dealuminized Beta

Despite the propensity for the formation of certain extra-framework Ti species, the demetallation-metalation method provides several advantages over traditional hydrothermal and dry-gel conversion methods. These advantages include high metal loading, high synthesis efficiency, and the easy incorporation of metal atoms with a large radius (Bregante and Flaherty, 2017; Li and Yu, 2021; Zhang et al., 2022). Moreover, compared with conventional hydrothermal titanosilicalites, the Ti-beta synthesized by demetallation-metalation method with more Ti species on external surfaces (Pan et al., 2022) showed superior reaction performances in 1-hexene epoxidation as shown in Fig. S2.

During demetallation-metalation process, Beta zeolites will firstly form hydrogen-bonded silanols group on defect sites such as hydroxyl nests after dealuminized process. Subsequently, the silanol defects (vacant T sites) are filled with Ti precursor, effectively repairing the surface vacant T sites. The chlorotitanate precursors ($TiCl_4$) dissolved in ethanol undergo dechlorination through ethoxy, leading to the formation of ethoxylated chlorotitanate ($(Ti(Cl)_{4-n}(OEt)_n)$) precursor and HCl (Liang et al., 2021a; Liang et al., 2021b). The evaporated ammonia in this strategy will react with HCl to synthesize NH_4Cl, which could be precipitated from ethanol, disrupting the reaction equilibrium and facilitating the substitution of Cl in chlorotitanate by ethanol, as illustrated in Fig. 1.

Thermal gravimetric mass spectrometry (TG-MS) was employed to examine the dynamic evolution of Ti precursor (Fig. 2a and b). Con-

band at 300–500 °C, attributed to the decomposition of NH_4Cl cerning the HCl signal, the ammonia-regulated Ti precursor exhibits a (Zelenková and Slovák, 2022; Zhang et al., 2012). Simultaneously, the

band at 100 °C is associated with the HCl formed by the reaction between $TiCl_4$ and ethanol.

The gradual shift of the ethanol signal from approximately 150 °C to 100 °C indicates the profound substitution of the Ti precursor by ethoxy. Additionally, the CO_2 signal arises from the combustion of ethanol/ethoxy (Liang et al., 2021b). The CO_2 signal at lower temperatures is

ascribed to ethanol, while the CO_2 signal at higher temperatures corresponds to ethoxy in ethoxylated chlorotitanate. In comparison with

(100–150 °C) of the ammonia-regulated Ti precursor is significantly the conventional Ti precursor, the CO_2 signal at low temperatures reduced, and the CO_2 signal at high temperatures gradually shifts to

even higher temperatures. These results highlight that ammonia facilitates the synthesis of deeply substituted Ti precursors by ethoxy groups.

The UV–vis spectra of hydrolyzed ammonia-regulated and conventional Ti precursors were utilized to assess the formation ability of TiO_x species (Fig. 2c) (Lin et al., 2021). It was observed that the ammonia-regulated Ti precursor significantly inhibits TiO_x formation and enhances the presence of Ti^{4+} species compared to conventional Ti precursors. The Ti species resulting from the dealumination-metallization process in ammonia-regulated N-Ti-beta and conventional Ti-beta solid samples were examined through DR UV–vis spectra (Fig. 2e and f). The Ti species on Ti-beta samples were typically categorized into four components: $Ti(OSi)_4$ (~200 nm), $Ti(OSi)_3(OH)$ (~220 to 235 nm), *hexa*-coordinated Ti (270 nm), and anatase TiO_2 (330 nm) species (Blasco et al., 1993; Song et al., 2023; Wang et al., 2023). It was observed that N-Ti-beta samples (13.4 %) exhibited a lower presence of anatase TiO_2 species compared to Ti-beta samples (19.6 %).

Fourier-transform infrared (FT-IR) spectroscopy (Fig. S3) provides

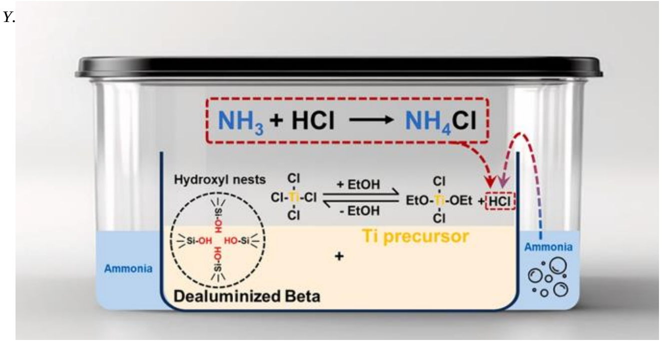

Fig. 1. The schematic diagram of ammonia-regulated evolution of Ti precursor and further incorporation into the framework of dealuminized Beta.

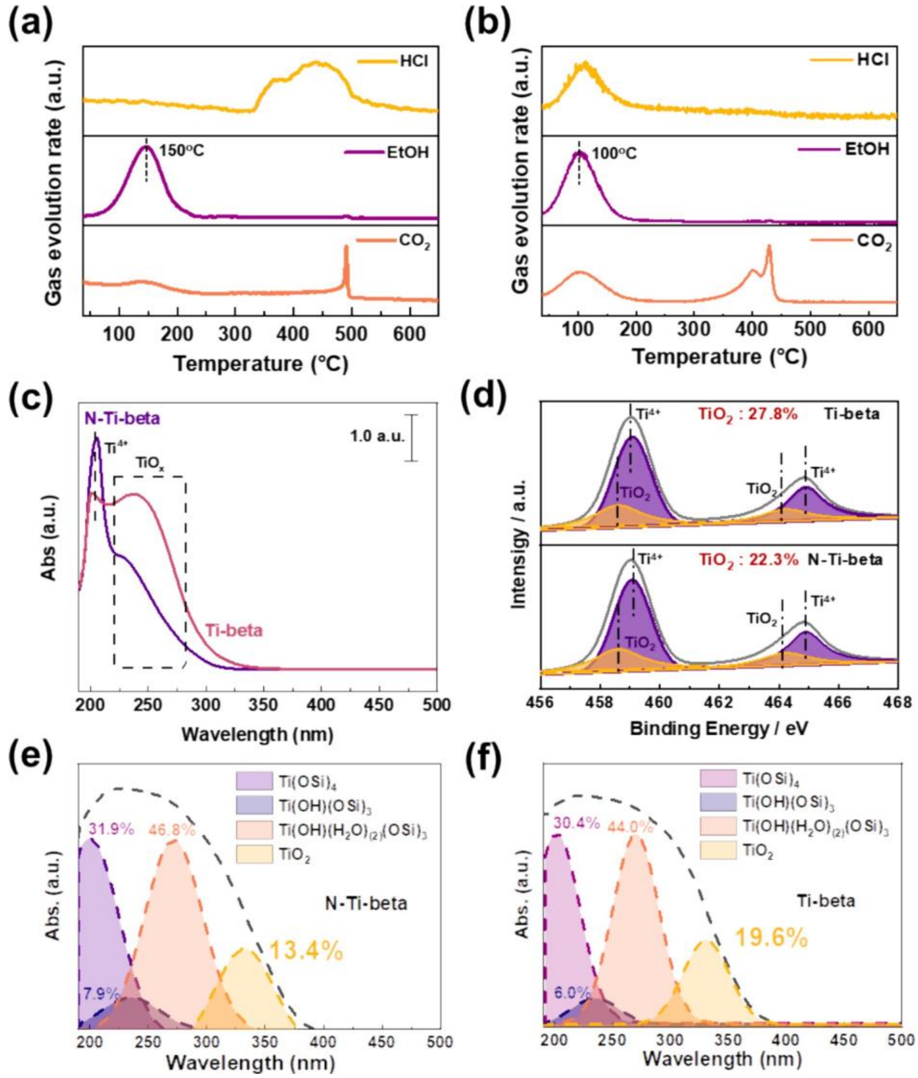

Fig. 2. TG-MS analysis results of (a) ammonia-regulated and (b) conventional Ti precursor supported on dealuminized Beta. (c) UV−vis spectra of hydrolyzed ammonia-regulated and conventional hydrolyzed Ti precursor. (d) XPS analysis of N-Ti-beta and Ti-beta samples in Ti(2p) regions. Diffuse reflectance (DR) UV−vis spectra of (e) ammonia-regulated N-Ti-beta and (f) conventional Ti-beta samples.

additional insights into the beta framework of N-Ti-beta and Ti-beta

1237 cm^{-1}. (He et al., 2015; Lin et al., 2022) Furthermore, the presence of a peak at 960 cm^{-1} serves as additional confirmation of the frame-samples, evident from the emergence of peaks at 530, 574, 624, and work Ti species in both N-Ti-beta and Ti-beta samples (Carati et al., 1999). The X-ray photoelectron spectroscopy (XPS) results further elucidate the Ti coordination states in different Ti-beta samples (Fig. 2d). Peaks at ~ 458.6 and 464.0/464.1 eV were attributed to TiO_2 species, while peaks at ~ 459.0/459.1 eV (Ti $2p_{3/2}$) and ~ 464.9 eV (Ti $2p_{1/2}$) were associated with framework Ti species (Lewis et al., 2022; Xu et al., 2023). Moreover, N-Ti-beta samples (22.3 %) displayed a reduced presence of TiO_2 species compared to conventional Ti-beta samples (27.8 %). These findings underscore the effectiveness of ammonia-regulated Ti precursors in suppressing the formation of TiO_x species and subsequent TiO_2 species on Ti-beta samples. In addition, the pore structure of ammonia-regulated and conventional Ti-beta samples underwent examination through N_2 adsorption–desorption isotherms (Fig. 3a). This analysis revealed that ammonia-regulated Ti-beta exhibited a higher specific surface area (583〉 533 m^2/g) and a larger mesoporous volume (0.179 > 0.134 cm^3/g), as detailed in Tables S1.

These N_2 adsorption–desorption results further demonstrate that the evaporated ammonia not only reacts with HCl to synthesize NH_4Cl but also etches the beta framework to create mesopores.

3.2. 1-Hexene epoxidation over ammonia-regulated and conventional Ti-beta

In the 1-hexene epoxidation as shown in Fig. 3b, the N-Ti-beta catalyst exhibits a higher conversion rate (61.2 % > 46.6 %) compared to the Ti-beta catalyst. This enhanced conversion of 1-hexene can be attributed to an increase in accessible Ti sites resulting from a higher specific surface area and elevated levels of framework Ti species. Additionally, the heightened selectivity towards 1,2-epoxyhexane (98.1 % > 91.8 %) in Fig. 3c is a consequence of reduced TiO_2 contents, which could lead to the deep oxidation of 1,2-epoxyhexane products (Feng et al., 2021; Lin et al., 2023b). Furthermore, owing to the decreased TiO_2 contents and increased accessibility of Ti sites, the H_2O_2 utilization efficiency with N-Ti-beta catalysts has significantly risen to 93.3 %, surpassing that of conventional Ti-beta catalysts (72.5 %).

The apparent activation energy in Fig. 3d was evaluated for both the N-Ti-beta and Ti-beta catalysts, revealing comparable values (11.14 kJ/mol vs. 12.47 kJ/mol). This similarity indicates a shared reaction pathway for N-Ti-beta and Ti-beta catalysts. High-resolution transmission electron microscopy (HRTEM) images (Fig. S4) further

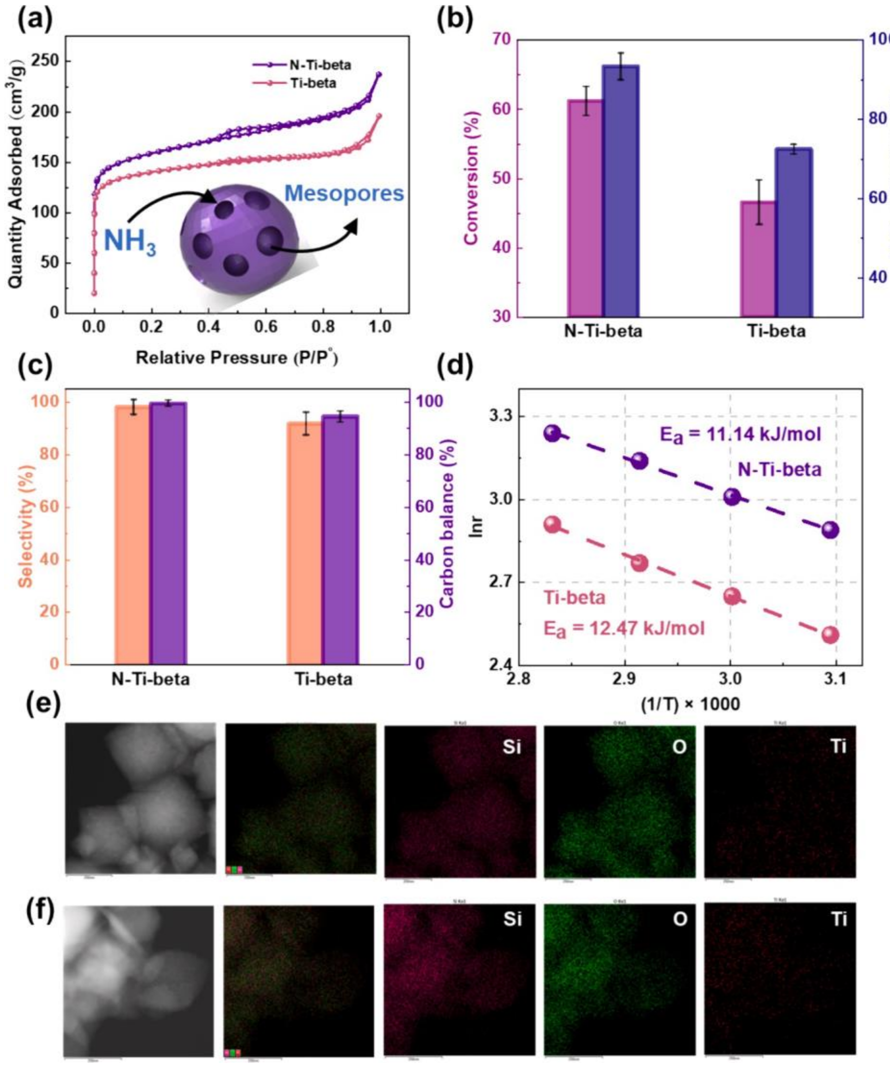

Fig. 3. (a) The N_2 adsorption–desorption isotherms of ammonia-regulated N-Ti-beta and conventional Ti-beta samples. (b) and (c) Catalytic reaction performances in 1-hexene epoxidation with ammonia-regulated N-Ti-beta and conventional Ti-beta samples. Reaction conditions: catalyst (0.2 g), CH_3CN (20 mL), H_2O_2 (30 wt%, 1.2 g), 1-hexene (1.2 g), reaction temperature (60 °C), reaction time (3 h), stirring rate (300 rpm). (d) Arrhenius plots over ammonia-regulated N-Ti-beta and conventional Ti-beta samples. The TEM-mapping of Si, O and Ti elements in (e) ammonia-regulated N-Ti-beta and (f) conventional Ti-beta samples.

underscore the analogous morphology, showcasing similar crystal planes (100). Additionally, TEM-mapping of Si, O, and Ti elements in N- Ti-beta and Ti-beta catalysts (Fig. 3e and f) reveals relatively uniform element distribution. These findings collectively affirm that the superior performance of N-Ti-beta catalysts in 1-hexene epoxidation should be attributed to the abundant framework Ti species and an increased accessibility of Ti sites.

Kinetic experiments were conducted to explore the difference on the 1-hexene epoxidation over ammonia-regulated N-Ti-beta and conventional Ti-beta catalysts. The turnover rate (TOR) for 1-hexene epoxidation, plotted against 1-hexene concentration, revealed consistently higher TOR values for N-Ti-beta catalysts compared to Ti-beta catalysts as 1-hexene concentration increased (Fig. 4a). Remarkably, as the 1-hexene concentration elevated from 2.41×10^{-2} to 11.08×10^{-2} M, both N-ranging from 4.26×10^{-3} to 17.07×10^{-3} and from 3.23×10^{-3} to 12.07 Ti-beta and Ti-beta catalysts exhibited a significant increase in TOR, $\times 10^{-3}$ mol $C_6H_{12}O$ (mol M·s)$^{-1}$, respectively. However, beyond a 1-hexene concentration of 11.08 M, TOR for both N-Ti-beta and Ti-beta remained nearly unchanged, indicating saturation of 1-hexene on the catalysts' surfaces. Furthermore, TOR for 1-hexene epoxidation, as a function of H_2O_2 concentration, revealed consistently higher values for ammonia-regulated N-Ti-beta catalysts compared to conventional Ti-as H_2O_2 concentration increased from 3.15×10^{-2} to 28.31×10^{-2} M, N-beta catalysts as H_2O_2 concentration increased (Fig. 4b). Interestingly, approximately ~ 1.4×10^{-2} and ~ 1.2×10^{-2} mol $C_6H_{12}O$ (mol M·s)$^{-1}$. Ti-beta and Ti-beta catalysts exhibited relatively stable TOR values at This signifies the remarkably efficient activation of H_2O_2 and enhanced saturation of H_2O_2 over Ti-beta catalysts, even at relatively low H_2O_2 concentrations.

The reaction orders for 1-hexene and H_2O_2 in the context of 1-hexene epoxidation were further examined. Notably, Fig. 4c illustrates that N-Ti-beta catalysts exhibited lower apparent reaction orders of 1-hexene (0.21) compared to Ti-beta catalysts (0.62). This disparity in reaction orders suggests that the reaction order for 1-hexene is notably lower over N-Ti-beta catalysts, indicating a higher degree of saturation of 1- hexene on their surfaces (Liu et al., 2023). The heightened 1-hexene adsorption observed with N-Ti-beta catalysts can be attributed to an increased specific surface area, facilitating greater accessibility to Ti sites. However, in Fig. 4d, it is observed that both N-Ti-beta and Ti-beta catalysts displayed similar apparent reaction orders (0.092 vs 0.096). The nearly zero order of H_2O_2 over both catalysts suggests that H_2O_2 and related active species are nearly fully saturated on the catalysts' surfaces. These findings reveal that while H_2O_2 and related active intermediates are nearly saturated for both catalysts, the enhanced 1-

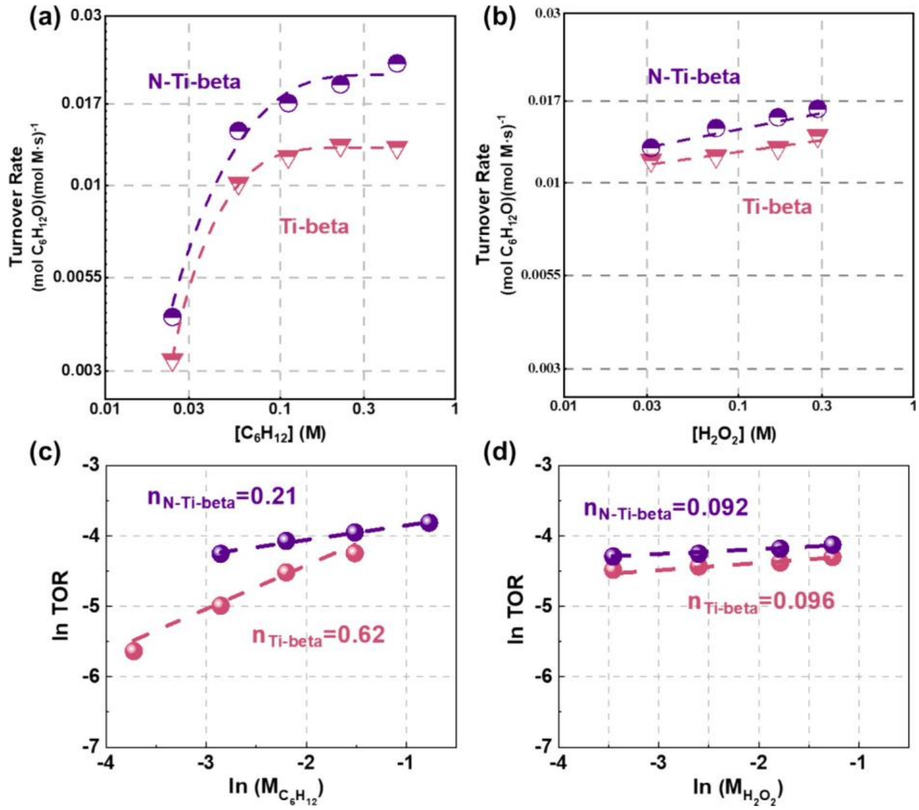

Fig. 4. Turnover rate for 1-hexene epoxidation over ammonia-regulated N-Ti-beta and conventional Ti-beta catalysts as a function of (a) 1-hexene and (b) H_2O_2 concentration. Prediction of kinetic reaction order for (c) 1-hexene and (d) H_2O_2 over ammonia-regulated N-Ti-beta and conventional Ti-beta catalysts.

hexene adsorption in N-Ti-beta catalysts which can be attributed to their increased specific surface area could effectively improve 1-hexene epoxidation.

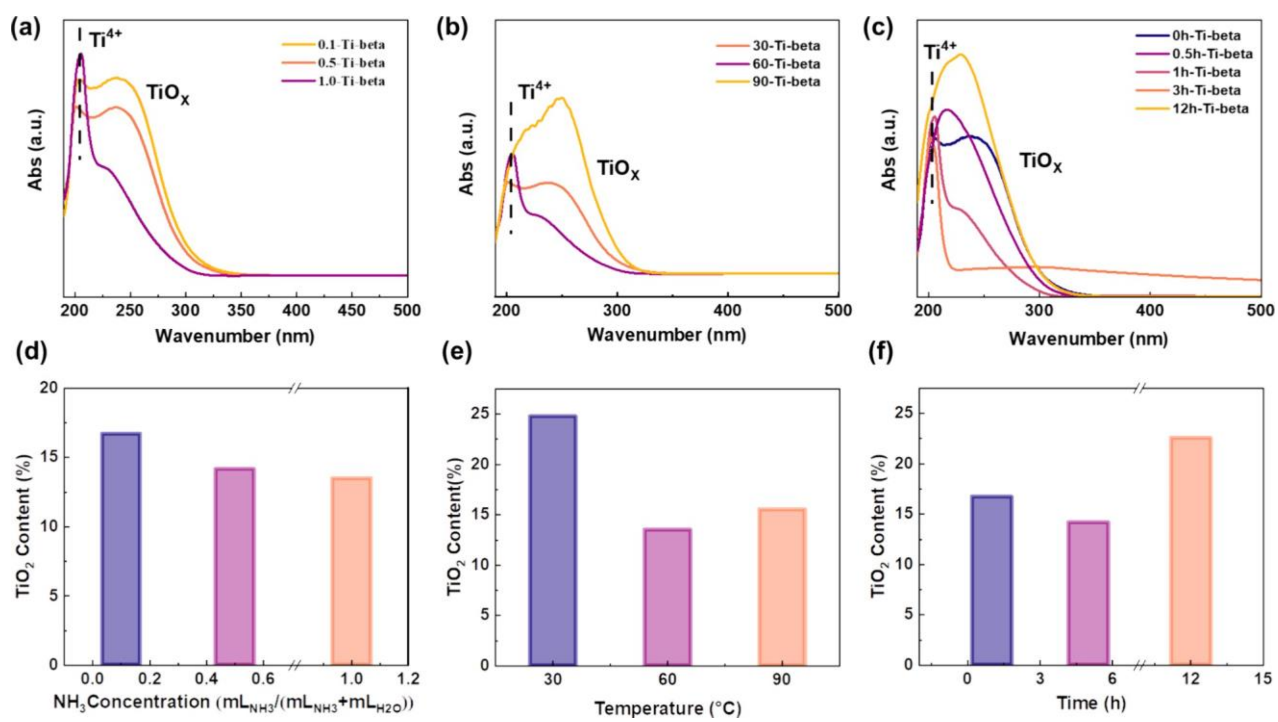

Fig. 5. UV–vis spectra of hydrolyzed ammonia-regulated Ti precursors at (a) different ammonia concentration, (b) different pretreatment temperatures (30 °C, 60 °C and 90 °C) and (c) different pretreatment time (0, 0.5, 1, 3 and 12 h). TiO_2 contents determined by UV–vis spectra in Ti-beta pretreated at (d) different ammonia concentration, (e) different pretreatment temperatures and (f) different pretreatment time.

3.3. *Effect of ammonia-regulated conditions over Ti-beta for 1-hexene epoxidation*

The ammonia concentration, pretreatment temperature and pretreatment time were optimized to investigate the effect of pretreatment conditions for the ammonia-regulated process on Ti-beta samples. The UV–vis spectra of hydrolyzed ammonia-regulated Ti precursors were employed to evaluate the formation capability of TiO_x species. It was noted that the concentration of TiO_x species exhibited a gradual decline with increasing ammonia concentration (Fig. 5a). The Ti species, arising from the dealumination-metallization process in ammonia-regulated N-Ti-beta, were further analyzed using DR UV–vis spectra (Fig. S5). The results indicated a progressive decrease in TiO_2 content, dropping from 16.7 % to 13.5 % as the ammonia concentration increased (Fig. 5d). This implies that an increased concentration of ammonia could enhance the substitution of Ti precursors with ethoxy groups to a greater extent, thus restraining the TiO_2 formation. The N_2 adsorption–desorption isotherms of N-Ti-beta samples at various ammonia concentrations revealed that the pore structure remained nearly unchanged (Fig. S6). Specifically, the 0.1-Ti-beta, 0.5-Ti-beta, and 1.0-Ti-beta exhibited nearly identical specific surface areas of approximately 591.2, 588.7, and 591.2 m^2/g, respectively.

The temperature was further optimized for the ammonia-regulated

TiO_x species exhibited a decline from 30 to 60 °C, followed by a significant increase from 60 to 90 °C (Fig. 5b). The TiO_2 contents in process of Ti-beta samples. It was observed that the concentration of different Ti-beta samples mirrored the trend of TiO_x species in Ti precursors (see Fig. S7). Specifically, the 60-Ti-beta showed the least TiO_2 content (13.5 %) compared to the other two catalysts (30-Ti-beta: 24.8

temperature (i.e., 60 °C) enhances NH_3 evaporation, facilitating its re- % and 90-Ti-beta: 15.6 %), as illustrated in Fig. 5e. Slightly raising the action with HCl to augment the substitution of Ti precursors by ethanol.

cies. Nevertheless, excessively high temperatures (i.e., 90 °C) lead to an Consequently, this contributes to an increase in the framework Ti speexcessive formation of NH_3. In this scenario, NH_3 not only reacts with HCl but also creates an alkaline environment, resulting in the formation of TiO_x species through the hydrolysis of Ti precursors. N_2 adsorp- tion–desorption isotherms of N-Ti-beta samples at different temperatures (Fig. S8) indicated that higher temperatures effectively induced the formation of mesopores. The 90-Ti-beta exhibited a typical type IV isotherm (Du et al., 2020; Feng et al., 2017), revealing a higher mesoporous volume (0.196 cm^3/g) compared to the 30-Ti-beta (0.176 cm^3/g) and 60-Ti-beta (0.179 cm^3/g) samples.

The pretreatment time was further optimized for the ammonia-regulated process of Ti-beta samples. It was found that the concentration of TiO_x species gradually decreased from 0 to 3 h and then exhibited a significant increase at 12 h (Fig. 5c). The TiO_2 contents in different Ti-beta samples are consistent with the trend of TiO_x species in Ti precursors (Fig. S9). It is found that TiO_2 contents in N-Ti-beta also demonstrated an inverted volcano curve (Fig. 5f), aligning with the observations in Fig. 5c. Therefore, extending the pretreatment duration (e.g., 0–3 h) amplifies NH_3 evaporation, promoting its interaction with HCl to enhance the substitution of Ti precursors with ethanol. This leads to an augmentation of the framework Ti species. However, an excessively prolonged pretreatment time (i.e., 12 h) results in an excessive generation of NH_3. In such cases, NH_3 not only reacts with HCl but also generates an alkaline environment, leading to the formation of TiO_x species through the hydrolysis of Ti precursors. N_2 adsorption–desorption isotherms of N-Ti-beta samples at pretreatment time (Fig. S10) indicated that a longer pretreatment time effectively induced the formation of mesopores. The 12 h-Ti-beta exhibited a typical type IV isotherm, revealing the presence of mesopores.

In the context of 1-hexene epoxidation with different N-Ti-beta samples at different ammonia concentration, the 1.0-Ti-beta catalyst demonstrated superior performance compared to other catalysts (0.1-Ti-beta and 0.5-Ti-beta catalysts), exhibiting the highest conversion of 1-hexene (64.1 %) and H_2O_2 utilization efficiency (92.2 %) in Fig. 6a. This superiority should be attributed to a higher content of framework Ti species facilitating 1-hexene epoxidation, coupled with restrained TiO_2 species that could otherwise lead to the inefficient decomposition of H_2O_2 (Xiong et al., 2016). For the effect of different pretreatment temperatures, it is found that the 60-Ti-beta demonstrated the highest conversion of 1-hexene (61.2 %) and H_2O_2 utilization efficiency (93.3 %) in Fig. 6b, which is in line with the content of framework Ti species. With the increase of pretreatment time from 1 to 5 h, the conversion of 1-hexene and H_2O_2 utilization efficiency gradually increased from 47.1 % to 65.6 % and 80.4 % to 95.8 %, respectively (Fig. 6c). Subsequently, with a further increase of pretreatment time from 5 to 12 h, the conversion of 1-hexene and H_2O_2 utilization efficiency gradually decreased from 65.6 % to 36.2 % and 95.8 % to 60.3 %, respectively. This volcano curve is consistent with the evolution of TiO_x species and further formation of extra-framework Ti species.

These results indicate that increasing ammonia concentration effectively inhibits the formation of TiO_x species by producing a deeply substituted Ti precursor, which subsequently reduces the amount of TiO_2 species. Additionally, raising the temperature of the ammonia appropriately further prevents the formation of TiO_x species, leading to a decrease in TiO_2 species. A longer pretreatment time can also restrain TiO_2 formation and increase mesoporous volume. However, excessively long pretreatment times may promote the formation of TiO_x and TiO_2 species due to interactions with Ti precursors and excessive NH_3.

Therefore, these pretreatment parameters (ammonia concentration, pretreatment temperature, and duration) significantly impact both the reaction between ammonia and HCl to produce NH_4Cl and the interaction between NH_3 and hydrolyzed Ti precursors, as shown in Fig. 6d. The former can disrupt the reaction equilibrium, promoting the substitution of Cl in chlorotitanate with ethanol to enhance Ti incorporation. In contrast, the latter can create an alkaline environment, leading to the formation of TiO_x species and mesopores. Hence, the Ti-beta with rich framework Ti species and mesopores could effectively enhance 1-hexene epoxidation.

4. Conclusion

In this paper, we present a unique ammonia-regulated approach aimed at regulating the evolution of Ti precursors to enhance the metalation of Ti atoms within dealuminized beta zeolites. This method involves the reaction of ammonia with HCl, resulting in the production of NH_4Cl. This disrupts the reaction balance and facilitates the substitution of Cl in chlorotitanate by ethanol. The resultant deeply substituted Ti precursor proves to be effective in restraining the formation of TiO_x and extra-framework TiO_2 species. Furthermore, the evaporation of NH_3 generates mesopores under optimized reaction conditions, enhancing the kinetic adsorption of macromolecular 1-hexene. The proposed optimized pretreatment conditions, specifically at 60 °C for 5 h with 100 % ammonia concentration, are suggested to effectively restrain the formation of TiO_x precursors through deeply substituted ethoxylated chlorotitanate ($Ti(Cl)_{4-n}(OEt)_n$) and enhance the kinetic adsorption of 1-hexene by increasing Ti accessible sites. The resulting synthesized ammonia-regulated N-Ti-beta demonstrates significantly improved 1-hexene epoxidation performance, boasting a conversion rate of 61 %, selectivity of 98 %, and a high H_2O_2 utilization efficiency of 93 %. This study not only introduces a novel approach to dynamically regulate the demetalation-metalation method through evolving Ti precursors with ammonia but also holds promise for advancing related industrial processes in demetalation-metalation methods.

CRediT authorship contribution statement

Yang Xu: Writing – original draft, Conceptualization. **Dong Lin:** Writing – review & editing, Writing – original draft, Conceptualization. **Ze Zong:** Investigation. **Qiuming He:** Investigation. **Zhe Ma:**

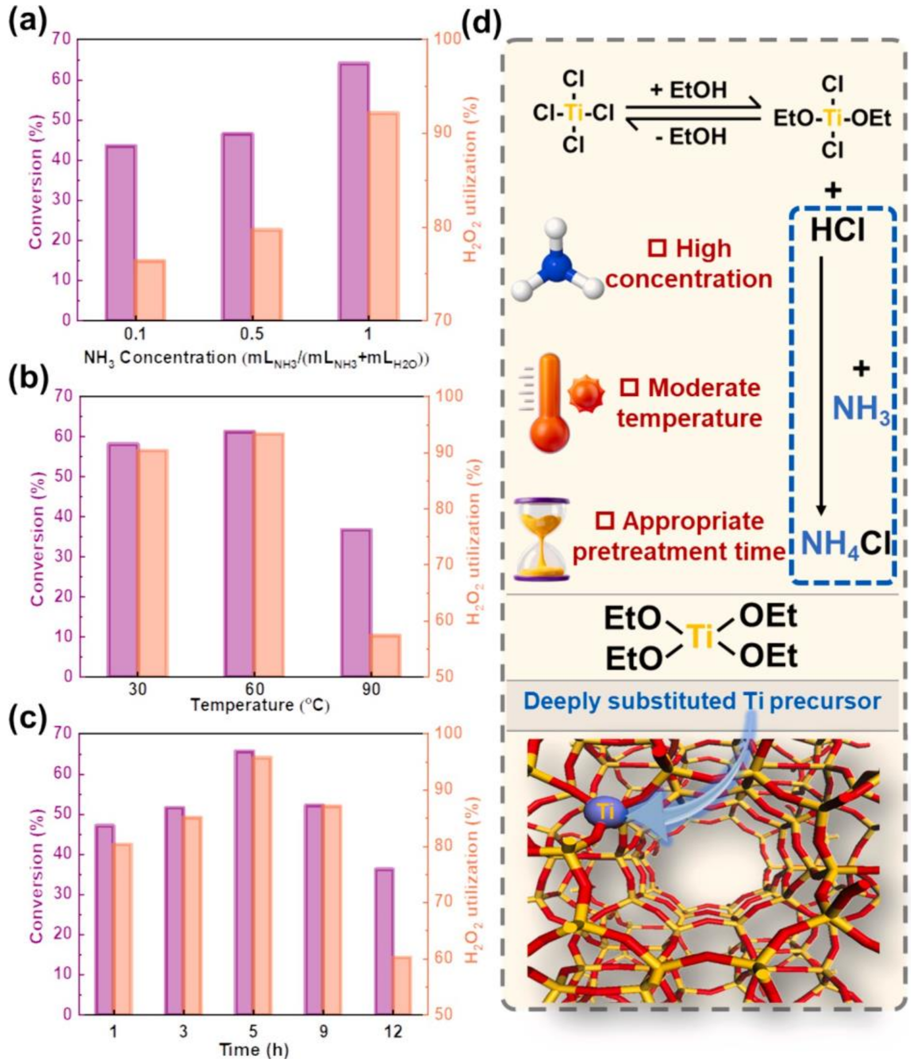

pretreatment time. Reaction conditions: catalyst (0.2 g), CH_3CN (20 mL), H_2O_2 (30 wt%, 1.2 g), 1-hexene (1.2 g), reaction temperature (60 °C), reaction time (3 h),
Fig. 6. Reaction performances of different N-Ti-beta samples at (a) different ammonia concentration, (b) different pretreatment temperatures and (c) different stirring rate (300 rpm). (d) Schematic diagram of effect of different pretreatment conditions for the framework Ti species.

Investigation. **Xuliang Deng:** Investigation. **De Chen:** Supervision, Funding acquisition. **Chaohe Yang:** Supervision, Funding acquisition, Formal analysis. **Xiang Feng:** Supervision, Funding acquisition, Formal analysis.

Declaration of competing interest

The authors declare that they have no known competing financial interests or personal relationships that could have appeared to influence the work reported in this paper.

Data availability

Data will be made available on request.

Acknowledgments

This work was supported by the National Natural Science Foundation of China-Outstanding Youth foundation (No. 22322814), National Natural Science Foundation of China (No. 22108307, No. 22108305), the National Natural Foundation of Shandong Province (ZR2021QB076, ZR2020YQ17, ZR2020KB006, ZR2023YQ009 and ZR2022MB015) and the Fundamental Research Funds for the Central Universities (23CX04029A).

References

Blasco, T., Camblor, M., Corma, A., Perez-Pariente,, 1993. The state of Ti in titanoaluminosilicates isomorphous with zeolite. beta. J. Am. Chem. Soc. 115, 11806–11813.
Bregante, D.T., Flaherty, D.W., 2017. Periodic trends in olefin epoxidation over group IV and V framework-substituted zeolite catalysts: a kinetic and spectroscopic study. J. Am. Chem. Soc. 139, 6888–6898.
Bregante, D.T., Thornburg, N.E., Notestein, J.M., Flaherty, D.W., 2018. Consequences of confinement for alkene epoxidation with hydrogen peroxide on highly dispersed group 4 and 5 metal oxide catalysts. ACS Catal. 8, 2995–3010.
Carati, A., Flego, C., Massara, E.P., Millini, R., Carluccio, L., Parker Jr, W., Bellussi, G., 1999. Stability of Ti in MFI and Beta structures: a comparative study. Microporous Mesoporous Mater. 30, 137–144.
Darensbourg, D.J., 2007. Making plastics from carbon dioxide: salen metal complexes as catalysts for the production of polycarbonates from epoxides and CO_2. Chem. Rev. 107, 2388–2410.
Deng, X., Yang, D., Li, W., Chai, Y., Wu, G., Li, L., 2023. Chemistry of coordinatively unsaturated centers in zeolites. Trends Chem.
Dijkmans, J., Gabri¨els, D., Dusselier, M., de Clippel, F., Vanelderen, P., Houthoofd, K., Malfliet, A., Pontikes, Y., Sels, B.F., 2013. Productive sugar isomerization with highly active Sn in dealuminated β zeolites. Green Chem. 15, 2777–2785.
Du, S., Chen, H.-M., Shen, H.-X., Chen, J., Li, C.-P., Du, M., 2020. Hierarchically nanoporous TS-1 zeolites for catalytic oxidation desulfurization of liquid fuels. ACS Appl. Nano Mater. 3, 9393–9400.

Feng, X., Sheng, N., Liu, Y., Chen, X., Chen, D., Yang, C., Zhou, X., 2017. Simultaneously enhanced stability and selectivity for propene epoxidation with H_2 and O_2 on Au catalysts supported on nano-crystalline mesoporous TS-1. ACS Catal. 7, 2668–2675.
Feng, X., Lin, D., Chen, D., Yang, C., 2021. Rationally constructed Ti sites of TS-1 for epoxidation reactions. Sci. Bull. 66, 1945–1949.
Ge, Z., Hu, H., Huang, Q., Chen, X., 2023. Synthesis of boron-free titanosilicate zeolite by $TiCl_4$/HCl treatment of pure silicon MWW as an epoxidation catalyst. J. Catal. 428, 115142.
Gordon, C.P., Engler, H., Tragl, A.S., Plodinec, M., Lunkenbein, T., Berkessel, A., Teles, J. H., Parvulescu, A.-N., Cop´eret, C., 2020. Efficient epoxidation over dinuclear sites in titanium silicalite-1. Nature 586, 708–713.
He, Z., Wu, J., Gao, B., He, H., 2015. Hydrothermal synthesis and characterization of aluminum-free Mn-β zeolite: a catalyst for phenol hydroxylation. ACS Appl. Mater. Interfaces 7, 2424–2432.
Hirahata, W., Thomas, R.M., Lobkovsky, E.B., Coates, G.W., 2008. Enantioselective polymerization of epoxides: a highly active and selective catalyst for the preparation of stereoregular polyethers and enantiopure epoxides. J. Am. Chem. Soc. 130, 17658–17659.
Lewis, R.J., Ueura, K., Liu, X., Fukuta, Y., Davies, T.E., Morgan, D.J., Chen, L., Qi, J., Singleton, J., Edwards, J.K., Freakley, S.J., Kiely, C.J., Yamamoto, Y., Hutchings, G. J., 2022. Highly efficient catalytic production of oximes from ketones using in situ–generated H_2O_2. Science 376, 615–620.
Li, Y., Yu, J., 2021. Emerging applications of zeolites in catalysis, separation and host–guest assembly. Nat. Rev. Mater. 6, 1156–1174.
Liang, X., Peng, X., Liu, D., Xia, C., Luo, Y., Shu, X., 2021a. Understanding the mechanism of N coordination on framework Ti of Ti-BEA zeolite and its promoting effect on alkene epoxidation reaction. Mol. Catal. 511, 111750.
Liang, X., Peng, X., Xia, C., Yuan, H., Zou, K., Huang, K., Lin, M., Zhu, B., Luo, Y., Shu, X., 2021b. Improving Ti incorporation into the BEA framework by employing ethoxylated chlorotitanate as Ti precursor: postsynthesis, characterization, and incorporation mechanism. Ind. Eng. Chem. Res. 60, 1219–1230.
Liang, Y., Xiong, C., Zhou, X., Xue, C., Ji, H., 2023. Preparation of Mo-based catalyst appreciated from agricultural waste for efficient high-value conversion of 1-hexene. Chem. Eng. J. 455, 140648.
Lin, D., Feng, X., Zheng, X., Xu, Y., Zhao, H., Song, Z., Wang, L., Shan, H., Xiao, F.S., Chen, D., Chaohe, Y., 2023a. Dimensional Regulation of Titanosilicate by Kinetically Controlled Intergrowth Crystals. Adv. Funct. Mater. 33, 2301179.
Lin, H., Wang, J., Gao, B., Yang, K., Lv, G., Qi, S., Zhu, Z., Lue, H., 2022. Solvent-free and low template content synthesis of Ti-Beta zeolite via interzeolite transformation for oxidative desulfurization. Microporous Mesoporous Mater. 344, 112203.
Lin, D., Zhang, Q., Qin, Z., Li, Q., Feng, X., Song, Z., Cai, Z., Liu, Y., Chen, X., Chen, D., Chaohe, Y., 2021. Reversing titanium oligomer formation towards high-efficiency and green synthesis of titanium-containing molecular sieves. Angew. Chem. Int. Ed. 60, 3443–3448.
Lin, D., Xu, Y., Zheng, X., Sheng, W., Liu, Z., Yan, Y., Cao, Y., Liu, Y., Feng, X., Chen, D., Chaohe, Y., 2023b. Engineering sodium-decorated bifunctional Au-Ti sites to boost molecular transfer for propene epoxidation with H_2 and O_2. AIChE J. 69, e17999.
Liu, Y., Liu, Z., Hui, Y., Wang, L., Zhang, J., Yi, X., Chen, W., Wang, C., Wang, H., Qin, Y., 2023. Rhodium nanoparticles supported on silanol-rich zeolites beyond the homogeneous Wilkinson's catalyst for hydroformylation of olefins. Nat. Commun. 14, 2531.
Liu, M., Wei, H., Li, B., Song, L., Zhao, S., Niu, C., Jia, C., Wang, X., Wen, Y., 2018. Green and efficient preparation of hollow titanium silicalite-1 by using recycled mother liquid. Chem. Eng. J. 331, 194–202.
Meng, X., Jin, F., qiang Peng, A., Jiang, X., Guo, X., Wu, G.,, 2024. Influence of different Ga species in MWW zeolite bifunctional catalysts on the ethane dehydrogenation and dehydroaromatization in the absence and presence of CO_2. Fuel 363, 130968.
Pan, H., Peng, R., Zhu, Z., Xu, H., He, M., Wu, P., 2022. Highly Hydrophilic Ti— Beta Zeolite with Ti— Rich Exterior as Efficient Catalyst for Cyclohexene Epoxidation. Catalysts 12, 434.
Pang, T., Yang, X., Yuan, C., Elzatahry, A.A., Alghamdi, A., He, X., Cheng, X., Deng, Y., 2021. Recent advance in synthesis and application of heteroatom zeolites. Chin. Chem. Lett. 32, 328–338.
Potts, D.S., Jeyaraj, V.S., Kwon, O., Ghosh, R., Mironenko, A.V., Flaherty, D.W., 2022. Effect of Interactions between Alkyl Chains and Solvent Structures on Lewis Acid Catalyzed Epoxidations. ACS Catal. 12, 13372–13393.
Rodríguez-Fern´andez, A., Di Iorio, J.R., Paris, C., Boronat, M., Corma, A., Rom´an-Leshkov, Y., Moliner, M., 2020. Selective active site placement in Lewis acid zeolites and implications for catalysis of oxygenated compounds. Chem. Sci. 11, 10225–10235.
Song, S., Di, L., Wu, G., Dai, W., Guan, N., Li, L., 2017. Meso-Zr-Al-beta zeolite as a robust catalyst for cascade reactions in biomass valorization. Appl. Catal. b: Environ. 205, 393–403.
Feng, X., 2023. Engineering a Coordinatively Unsaturated Au–O–Ti^{3+} Structure Song, Z., Yan, H., Yuan, J., Ma, H., Cao, J., Wang, Y., Wang, Q., Peng, C., Deng, F., Toward Unprecedented H_2 Efficiency for Low-Temperature Propene Epoxidation
with H_2 and O_2. Engineering.
Suib, S.L., Přech, J., Szaniawska, E., Čejka, J.i.,, 2022. Recent Advances in Tetra-(Ti, Sn, Zr, Hf) and Pentavalent (Nb, V, Ta) Metal-Substituted Molecular Sieve Catalysis. Chem. Rev. 123, 877–917.
Tan, J.Z., Bregante, D.T., Torres, C., Flaherty, D.W., 2022. Transition state stabilization depends on solvent identity, pore size, and hydrophilicity for epoxidations in zeolites. J. Catal. 405, 91–104.
Tang, B., Dai, W., Sun, X., Guan, N., Li, L., Hunger, M., 2014. A procedure for the preparation of Ti-Beta zeolites for catalytic epoxidation with hydrogen peroxide. Green Chem. 16, 2281–2291.
Wang, B., Guo, Y., Zhu, J., Ma, J., Qin, Q., 2023. A review on titanosilicate-1 (TS-1) catalysts: Research progress of regulating titanium species. Coord. Chem. Rev. 476, 214931.
Wolf, P., Hammond, C., Conrad, S., Hermans, I., 2014. Post-synthetic preparation of Sn-, Ti-and Zr-beta: a facile route to water tolerant, highly active Lewis acidic zeolites. Dalton Trans. 43, 4514–4519.
Xiong, G., Cao, Y., Guo, Z., Jia, Q., Tian, F., Liu, L., 2016. The roles of different titanium species in TS-1 zeolite in propylene epoxidation studied by in situ UV Raman spectroscopy. Phys. Chem. Chem. Phys. 18, 190–196.
Xu, J., Zhang, Z., Yu, D., Du, W., Song, N., Duan, X., Zhou, X., 2023. Au/TS-1 catalyst for propylene epoxidation with H_2 and O_2: Effect of surface property and morphology of TS-1 zeolite. Nano Res. 16, 6278–6289.
Yamagishi, K., Namba, S., Yashima, T., 1991. Defect sites in highly siliceous HZSM-5 zeolites: a study performed by alumination and IR spectroscopy. J. Phys. Chem. 95, 872–877.
Yuan, J., Fu, R., Fan, L., Dong, Y., Zong, Z., Kang, H., Yan, H., Liu, Y., Zhang, X., Zhao, G., Xuliang, D., Yongjun, Z., Jincheng, L., Chaohe, Y., Honghong, S., De, C., Xiang, F., 2023. Silica islands regulated external Ti-site environment of TS-1 for enhanced performance of 1-hexene epoxidation. AIChE J. 69, e17955.
Zelenkov´a, G., Slova´k, V., 2022. Decomposition of ammonium salts by quantitative TG-MS. J. Therm. Anal. Calorim. 147, 15059–15068.
Zhang, Q., Gao, S., Yu, J., 2022. Metal sites in zeolites: Synthesis, characterization, and catalysis. Chem. Rev. 123, 6039–6106.
Zhang, M., Ren, S., Guo, Q., Shen, B., 2021. Synthesis of hierarchically porous zeolite TS-1 with small crystal size and its performance of 1-hexene epoxidation reaction. Microporous Mesoporous Mater. 326, 111395.
Zhang, J., Zhang, R., Geerlings, H., Bi, J., 2012. Mg-Silicate Carbonation Based on an HCl-and NH_3-Recyclable Process: Effect of Carbonation Temperature. Chem. Eng. Technol. 35, 525–531.
Zhao, G., Deng, X., Lin, D., Liu, J., Zhang, Y.-J., Liu, Y., Chen, X., Feng, X., Chen, D., Yang, C., 2023. Constructing Highly Efficient Ti Sites of TS-1 for Alkene Epoxidation. Ind. Eng. Chem. Res. 62, 18205–18229.